Research article JHEP|Reports

Spatial molecular and cellular determinants of STAT3 activation in liver fibrosis progression in non-alcoholic fatty liver disease

Authors

Jingjing JiaoJessica I. Sanchez Omar A. Saldarriaga, Luisa M. Solis, David J. Tweardy, Dipen M. Maru, Heather L. Stevenson, Laura Beretta

Correspondence

lberetta@mdanderson.org (L. Beretta).

Graphical abstract

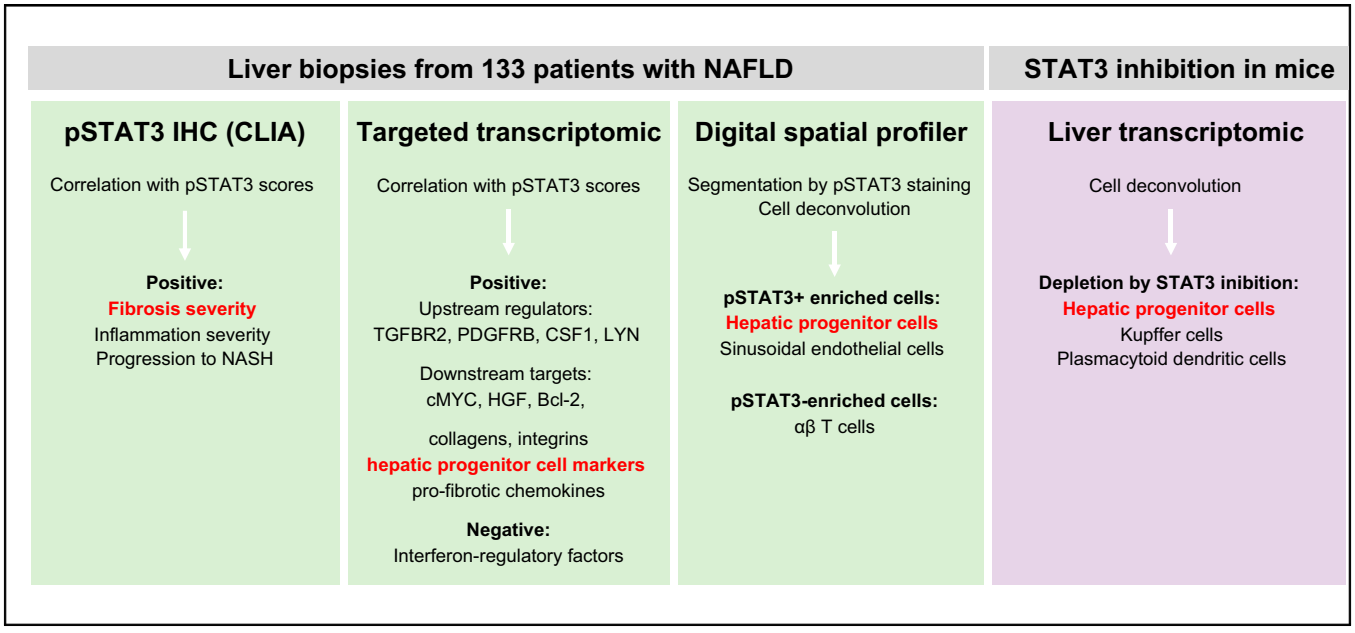

Highlights

- Advanced liver fibrosis is the main determinant of mortality in patients with NASH.
- Non-hepatocyte pSTAT3 in NAFLD liver biopsies correlated with fibrosis severity, inflammation and progression to NASH.
- PSTAT3 was enriched in HPCs and SECs as determined by digital spatial profiling of NASH biopsies.
- STAT3 inhibition in mice resulted in reduced liver fibrosis and depletion of HPCs, Kupffer cells and plasmacytoid DCs.
- In conclusion, STAT3 activation in HPCs results in their expansion and may mediate fibrogenesis in NAFLD.

Impact and implications

Advanced liver fibrosis is the main determinant of mortality in patients with NASH. This study showed using liver biopsies from 133 patients with NAFLD, that STAT3 activation in non-hepatocyte areas is strongly associated with fibrosis severity, inflammation, and progression to NASH. STAT3 activation was enriched in hepatic progenitor cells (HPCs) and sinusoidal endothelial cells (SECs), as determined by innovative technologies interrogating the spatial distribution of pSTAT3. Finally, STAT3 inhibition in mice resulted in reduced liver fibrosis and depletion of HPCs, suggesting that STAT3 activation in HPCs contributes to their expansion and fibrogenesis in NAFLD.

https://doi.org/10.1016/j.jhepr.2022.100628

Research article

JHEP|Reports

Spatial molecular and cellular determinants of STAT3 activation in liver fibrosis progression in non-alcoholic fatty liver disease

Jingjing Jiao,[1,†] **Jessica I. Sanchez,**[1,†] Omar A. Saldarriaga,[2] Luisa M. Solis,[3] David J. Tweardy,[4] Dipen M. Maru,[5] Heather L. Stevenson,[2] Laura Beretta[1,*]

[1]*Department of Molecular and Cellular Oncology, The University of Texas MD Anderson Cancer Center, Houston, TX, USA;* [2]*Department of Pathology, The University of Texas Medical Branch, Galveston TX, USA;* [3]*Department of Translational Molecular Pathology, The University of Texas MD Anderson Cancer Center, Houston, TX, USA;* [4]*Department of Infectious Diseases, Infection Control, and Employee Health, The University of Texas MD Anderson Cancer Center, Houston, TX, USA;* [5]*Department of Pathology, The University of Texas MD Anderson Cancer Center, Houston, TX, USA*

JHEP Reports **2023.** https://doi.org/10.1016/j.jhepr.2022.100628

Background & Aims: The prevalence of non-alcoholic fatty liver disease (NAFLD) and its severe form, non-alcoholic steatohepatitis (NASH), is increasing. Individuals with NASH often develop liver fibrosis and advanced liver fibrosis is the main determinant of mortality in individuals with NASH. We and others have reported that STAT3 contributes to liver fibrosis and hepatocellular carcinoma in mice.

Methods: Here, we explored whether STAT3 activation in hepatocyte and non-hepatocyte areas, measured by phospho-STAT3 (pSTAT3), is associated with liver fibrosis progression in 133 patients with NAFLD. We further characterized the molecular and cellular determinants of STAT3 activation by integrating spatial distribution and transcriptomic changes in fibrotic NAFLD livers.

Results: pSTAT3 scores in non-hepatocyte areas progressively increased with fibrosis severity ($r = 0.53$, $p < 0.001$). Correlation analyses between pSTAT3 scores and expression of 1,540 immune- and cancer-associated genes revealed a large effect of STAT3 activation on gene expression changes in non-hepatocyte areas and confirmed a major role for STAT3 activation in fibrogenesis. Digital spatial transcriptomic profiling was also performed on 13 regions selected in hepatocyte and non-hepatocyte areas from four NAFLD liver biopsies with advanced fibrosis, using a customized panel of markers including pSTAT3, PanCK+CK8/18, and CD45. The regions were further segmented based on positive or negative pSTAT3 staining. Cell deconvolution analysis revealed that activated STAT3 was enriched in hepatic progenitor cells (HPCs) and sinusoidal endothelial cells. Regression of liver fibrosis upon STAT3 inhibition in mice with NASH resulted in a reduction of HPCs, demonstrating a direct role for STAT3 in HPC expansion.

Conclusion: Increased understanding of the spatial dependence of STAT3 signaling in NASH and liver fibrosis progression could lead to novel targeted treatment approaches.

Impact and implications: Advanced liver fibrosis is the main determinant of mortality in patients with NASH. This study showed using liver biopsies from 133 patients with NAFLD, that STAT3 activation in non-hepatocyte areas is strongly associated with fibrosis severity, inflammation, and progression to NASH. STAT3 activation was enriched in hepatic progenitor cells (HPCs) and sinusoidal endothelial cells (SECs), as determined by innovative technologies interrogating the spatial distribution of pSTAT3. Finally, STAT3 inhibition in mice resulted in reduced liver fibrosis and depletion of HPCs, suggesting that STAT3 activation in HPCs contributes to their expansion and fibrogenesis in NAFLD.

Introduction

The prevalence of non-alcoholic fatty liver disease (NAFLD) is increasing in the US.[1] Non-alcoholic steatohepatitis (NASH), the severe form of NAFLD, is now the second most common indication for liver transplantation.[2] There is currently no approved therapy for NAFLD, although several drugs are in the advanced stages of development.[3] Liver fibrosis is the most important predictor of mortality in patients with NAFLD and a major risk factor for hepatocellular carcinoma (HCC).[4] The risk of liver-related mortality increases exponentially with fibrosis stage.[5,6] The age-adjusted prevalence of NAFLD with liver fibrosis F2–F4 in the US population is 4.4%, reaching 18.3% in those with type 2 diabetes.[7] It is therefore urgent to characterize in-depth the molecular mechanisms that contribute to liver fibrosis progression in NAFLD and develop novel surveillance and prevention strategies.

Signal transducer and activator of transcription 3 (STAT3) is a transcription factor that belongs to the Janus Kinase-STAT pathway. Phosphorylation at tyrosine Y705 is a key event in canonical STAT3 activation, with multiple upstream inputs that

Keywords: fibrosis; STAT3; NAFLD; NASH; cirrhosis; liver cancer.
Received 9 May 2022; received in revised form 3 November 2022; accepted 5 November 2022; available online 22 November 2022

† Contributed equally.

* Corresponding author. Address: Department of Molecular and Cellular Oncology, The University of Texas MD Anderson Cancer Center, Houston, USA. Tel.: 713-792-9100
E-mail address: lberetta@mdanderson.org (L. Beretta).

lead to the activation of STAT3.[8] STAT3 downstream target genes mediate STAT3's role in development, normal physiology, and pathology of many diseases, including cancers.[9] STAT3 activation was detected in all rodent models of liver injury[10] and in multiple human liver diseases, including steatosis,[11] fibrosis/cirrhosis,[12,13] and HCC.[14,15] We and others have shown that STAT3 activation contributes to HCC development and growth in NASH- and obesity-related mouse models.[16,17] We have also reported the therapeutic effect of a small-molecule STAT3 inhibitor, TTI-101 (previously named C188-9), in a preclinical model of NASH-related HCC.[17] STAT3 has therefore emerged as a promising target for pharmacological intervention in HCC and TTI-101 is currently in a phase I clinical trial for the treatment of HCC and other solid tumors. We also reported that the tumor growth inhibition was concomitant with improvements in steatosis, inflammation, fibrosis, and liver injury markers.[17] Other STAT3 inhibitors have also been reported to decrease liver fibrosis in preclinical models.[12,18] However, to date, no study has evaluated the activation of STAT3 and the spatial expression of activated STAT3 in liver fibrosis in patients with NAFLD. Thus, we explored whether STAT3 activation, estimated by levels of STAT3 phosphorylated on Y705 (pSTAT3), is associated with liver fibrosis severity, in a cohort of patients with histologically characterized NAFLD. We further investigated the spatial distribution of pSTAT3 and transcriptomic changes in fibrotic NAFLD livers to characterize the molecular and cellular determinants mediating STAT3-induced liver fibrosis.

Patients and methods

Patients and liver biopsy samples

Archived formalin-fixed paraffin-embedded (FFPE) liver biopsies from 133 patients with NAFLD, obtained through the percutaneous route using an 18-gauge core needle, were used for this study. Participants were recruited from The University of Texas Medical Branch at Galveston and written informed consent was obtained from each participant in the study. Demographic and clinical parameters from these patients are shown in Table S1. At collection, biopsies were immediately placed into 10% buffered formalin and processed using a TissueTekVIP tissue processor (Sakura Finetek, Torrance, CA) prior to being paraffin-embedded. Each biopsy was evaluated for fibrosis stage using the criteria reported by Brunt *et al.*[19] (F0: no fibrosis; F1: mild/moderate zone three perisinusoidal fibrosis or portal/periportal fibrosis only; F2: perisinusoidal and portal/periportal fibrosis; F3: bridging fibrosis; F4: cirrhosis) and components of the NAFLD activity score (NAS): steatosis (S0: <5%, S1: 5-33%, S2: >33-66%, S3: >66%), lobular inflammation (I0: no foci; I1: <2 foci per 200x field; I2: 2-4 foci per 200x field; I3: >4 foci per 200x field) and hepatocyte ballooning (B0: none; B1: few ballooning cells; B2: many cells with prominent ballooning). The study was conducted according to the guidelines of the Declaration of Helsinki and approved by the institutional review boards of the participating institutions.

IHC analysis of pSTAT3

Immunohistochemical (IHC) analysis was performed on an automated immunostainer (Leica Bond III IHC Stainer, San Diego, CA). Tissue sections (3 μm) were deparaffinized and underwent heat-induced antigen retrieval using the Tris-EDTA buffer for 20 min. Phospho-STAT3 on Tyr705 (pSTAT3) antibody (Cell Signaling #9145) was used at 1:100 dilution. Digital images were captured at 20x magnification using a whole slide scanner (Leica Aperio ImageScope software) and saved in SVS. format (Aperio). Portal triads and lobular inflammatory foci were annotated as non-hepatocyte areas. Liver lobular areas excluding inflammatory foci were annotated as hepatocyte areas. Quantification of pSTAT3 (pSTAT3 score) was developed in a CLIA laboratory, using nuclear V.9 algorithm (Aperio) and the product of the staining intensity multiplied by the percentage of nuclei ([3 × % of 3+ cells] + [2 × % of 2+ cells] + [1 × % of 1+ cells]).

RNA isolation and targeted gene expression profiling

FFPE tissue blocks were sectioned at a thickness of 3 μm (2-3 sections per block). RNA was extracted using the High Pure FFPET RNA Isolation kit (Roche). The concentration of the extracted RNA samples was measured with Qubit and quality control was performed on a bioanalyzer using RNA6000 pico assay. The percentage of RNA fragments above 200 nucleotides was used to adjust RNA input. Gene expression was interrogated using the PanCancer Immune Profiling and PanCancer Pathways panels (NanoString Technologies) in the nCounter® SPRINT platform. Gene expression data were analyzed using NanoString's software nSolver V.4.0 with Advanced Analysis 2.0 plugin. Data were normalized using the Advanced Analysis tool which draws on the NormqPCR R package.[20]

GeoMx DSP whole transcriptome workflow

Slides (4 μm) for four NAFLD liver biopsies with advanced fibrosis were submitted for digital spatial profiler (DSP) whole transcriptome sequencing (NanoString). The panel of morphology markers was custom designed to include pSTAT3 in addition to SYTO13 nuclear stain, PanCK+CK8/18, and CD45. Slides were stained with RNAscope probes and GeoMx DSP oligo-conjugated RNA detection probes and incubated overnight at 37 °C. Slides were then washed with equal parts of 4x saline sodium citrate (SSC) and 100% formamide, and dipped into 2xSSC-T (20xSSC, 10% tween-20) to allow coverslips to slide off. Slides were then washed with 2xSSC and transferred to a humidity chamber for antibody staining. Slides were covered with 200 μl Buffer W (GeoMx RNA slide prep kit, Nanostring) and incubated at room temperature for 30 min. Buffer W was removed and 200 μl of morphology marker solution was applied to each tissue. Slides were stained for 1 h in the humidity chamber at room temperature and then washed with 2xSSC. Slides were immediately loaded onto the GeoMX DSP slide holder with 6 ml of Buffer S (GeoMx RNA slide prep kit, Nanostring). Files were configured to associate RNA targets and GeoMx readout barcodes. The appropriate scan type and focus channel were selected to populate fluorescence exposure settings. Scan areas were defined for high magnification. A total of 13 regions of interest (ROIs) were selected including five non-hepatocyte and eight hepatocyte areas. The ROIs were further segmented based on pSTAT3-positive or -negative staining. The DSP barcodes were UV-cleaved and collected for each ROI and were subsequently dispensed into a 96-well plate and counted. During the library preparation, the DSP barcodes were tagged with their specific ROI location and RNA target identification sequence, thus matching them to their *in situ* hybridization probes and a unique molecular identifier to deduplicate reads. Sequenced oligonucleotides were then processed and imported back into the GeoMx DSP platform for integration with the slide images and ROI selections for spatially resolved RNA expression. FASTQ

sequencing files were processed into digital count conversion digital files using Nanostring's GeoMx NGS Pipeline software. Quality control checks and data analysis were performed in the GeoMx DSP Data Analysis suite. Data were filtered by the limit of quantitation and then normalized by the third quartile of all counts.

Cell deconvolution analyses

Cell deconvolution analyses were generated in the GeoMx DSP control center, using the spatialdecon geoscript (v1.1, updated April 2021) available at Nanostring's Geoscript Hub [https://nanostring.com/products/geomx-digital-spatial-profiler/geoscript-hub/]. The analyses were run using the landscape adult liver 10x matrix [https://github.com/Nanostring-Biostats/CellProfileLibrary].[21] CIBERSORTx [https://cibersortx.stanford.edu/] was used to generate cell deconvolution analyses using the adult mouse liver matrix [https://github.com/Nanostring-Biostats/CellProfileLibrary][22] and RNA-sequencing data from Hep*Pten*$^{-}$ NASH mouse livers treated with the STAT3 inhibitor C188-9 or placebo for 4 weeks and reported in.[17]

Statistical analyses

Principal component analysis was performed with Euclidian-based distance matrices, generated in R using log2-transformed gene expression values and log10-transformed expression values alongside permutational multivariate analysis of variance test for statistical significance. QIAGEN's Ingenuity® Pathway Analysis (IPA) core analysis was performed on fibrosis-correlated genes associated with STAT3 activation. Scatter plots and cell deconvolution plots were generated in Graph Prism 9.0.0.

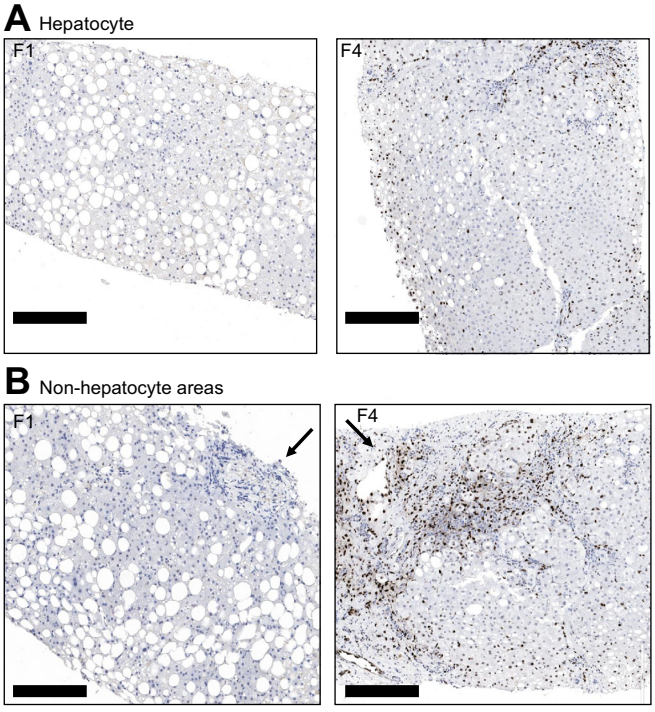

Fig. 1. Nuclear staining of pSTAT3. (A) In hepatocytes, and (B) in non-hepatocyte areas, of representative liver biopsies from patients with NAFLD. Scale bar: 200 Mm. NAFLD, non-alcoholic fatty liver disease; pSTAT3, phospho-STAT3.

Results

Characteristics of individuals with NAFLD

The demographic and clinical parameters of the 133 patients with NAFLD included in the study are summarized in Table S1. The patients had a median age of 51 years and were predominantly females (65%). The large majority were obese (89%) with a median BMI of 41.5, and 48% had type 2 diabetes. The majority were White with 67% non-Hispanic White and 25% Hispanics. The distribution of liver fibrosis stages was 2% F0, 33% F1, 28% F2, 14% F3, and 23% F4. Thirty-seven percent of participants had mild steatosis (S1), 43% had moderate steatosis (S2) and 15% had marked steatosis (S3). Of note, 4% of participants had cirrhosis and burned-out NASH. The proportion of patients with no ballooning (B0), few ballooning cells (B1), and prominent ballooning (B2) was 32%, 51%, and 15%, respectively. The proportion of patients with no lobular inflammation (I0), mild inflammation (I1), moderate inflammation (I2), and strong inflammation (I3) was 3%, 47%, 44%, and 5%, respectively.

Hepatic STAT3 activation and liver fibrosis severity

We first examined the relationship between liver histology features and hepatic levels of STAT3 phosphorylation at tyrosine 705 (pSTAT3), a measurement of STAT3 activation. pSTAT3 staining was observed in both hepatocyte and non-hepatocyte areas (Fig. 1). pSTAT3 staining was successfully scored in hepatocyte and non-hepatocyte areas, in 126 biopsies. While pSTAT3 scores in hepatocytes did not significantly differ between liver fibrosis stages, with a median ranging from 2.25 to 10.53, a small positive correlation was observed between hepatocyte pSTAT3 scores and liver fibrosis stages (r = 0.24, p = 0.034) (Fig. 2A, upper panel). In contrast, non-hepatocyte pSTAT3 scores significantly increased with fibrosis severity (Fig. 2A, lower panel). The median non-hepatocyte pSTAT3 scores were 4.68 in F1, 8.52 in F2, 11.33 in F3, and 13.69 in F4 (p <0.001). These results were further confirmed by a strong positive correlation between non-hepatocyte pSTAT3 scores and liver fibrosis stages (r = 0.53, p <0.001). Non-hepatocyte pSTAT3 scores were also significantly higher in patients with NASH compared to patients with NAFLD without NASH (11.04 *vs.* 5.72, p = 0.017) (Fig. 2B, lower panel). This result was confirmed by Spearman correlation analysis, as NAS and non-hepatocyte pSTAT3 scores positively correlated (r = 0.22, p = 0.05). While no significant changes in non-hepatocyte pSTAT3 scores were observed with steatosis severity (Fig. 2C, lower panel), non-hepatocyte pSTAT3 scores positively correlated with inflammation severity (r = 0.34, p = 0.002) (Fig. 2D, lower panel) and ballooning (r=0.25, p = 0.02) (Fig. 2E, lower panel). Non-hepatocyte pSTAT3 scores increased with inflammation severity from 5.37 in participants with inflammation scores I0-1, to 11.04 in those with I2 and 18.94 with I3 (p = 0.005) (Fig. 2D, lower panel). Patients with prominent ballooning (B2) had higher non-hepatocyte pSTAT3 scores (16.88) compared to those with no ballooning (B0, 5.78) or mild ballooning (B1, 9.04) (p = 0.020) (Fig. 2E, lower panel). There was no significant difference in hepatocyte pSTAT3 scores with NASH or severity of steatosis, ballooning, and inflammation (Fig. 2B-E, upper panels).

Hepatic gene expression changes associated with STAT3 activation in patients with NAFLD

Using the targeted PanCancer Immune Profiling and PanCancer Pathways panels, the expression of 770 immune-related genes

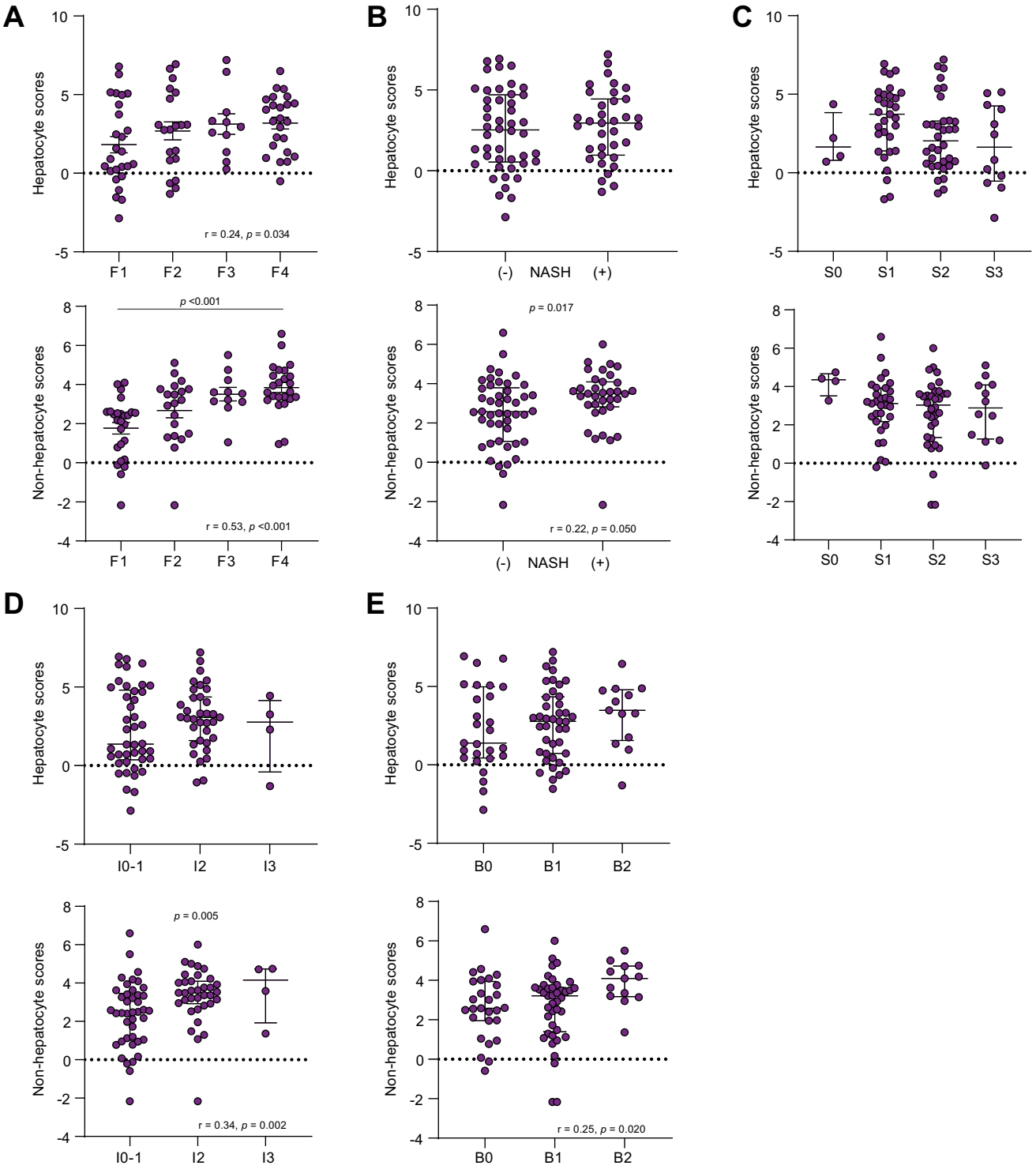

Fig. 2. Quantification of pSTAT3 nuclear staining in hepatocytes (top) and non-hepatocyte areas (bottom) in liver biopsies. (A) With F1 to F4 fibrosis stages. (B) With or without NASH. (C) With different degrees of steatosis. (D) With different degrees of inflammation. (E) With different degrees of ballooning. Log2-transformed pSTAT3 scores were used. Error bar: interquartile range. Statistical significance was calculated using Kruskal–Wallis test (more than two groups) or Mann-Whitney test (two groups). NASH, non-alcoholic steatohepatitis; pSTAT3, phospho-STAT3.

and of 770 genes related to cancer-associated canonical pathways was successfully measured in RNA extracted from 101 of the same archived liver biopsies. To determine the contribution of STAT3 activation to the fibrogenic process in NAFLD, Spearman correlation analyses were performed between expression levels of these genes and pSTAT3 scores. A total of 120 genes and 319 genes positively correlated with hepatocyte and non-hepatocyte pSTAT3 scores, respectively, including 54 genes in common

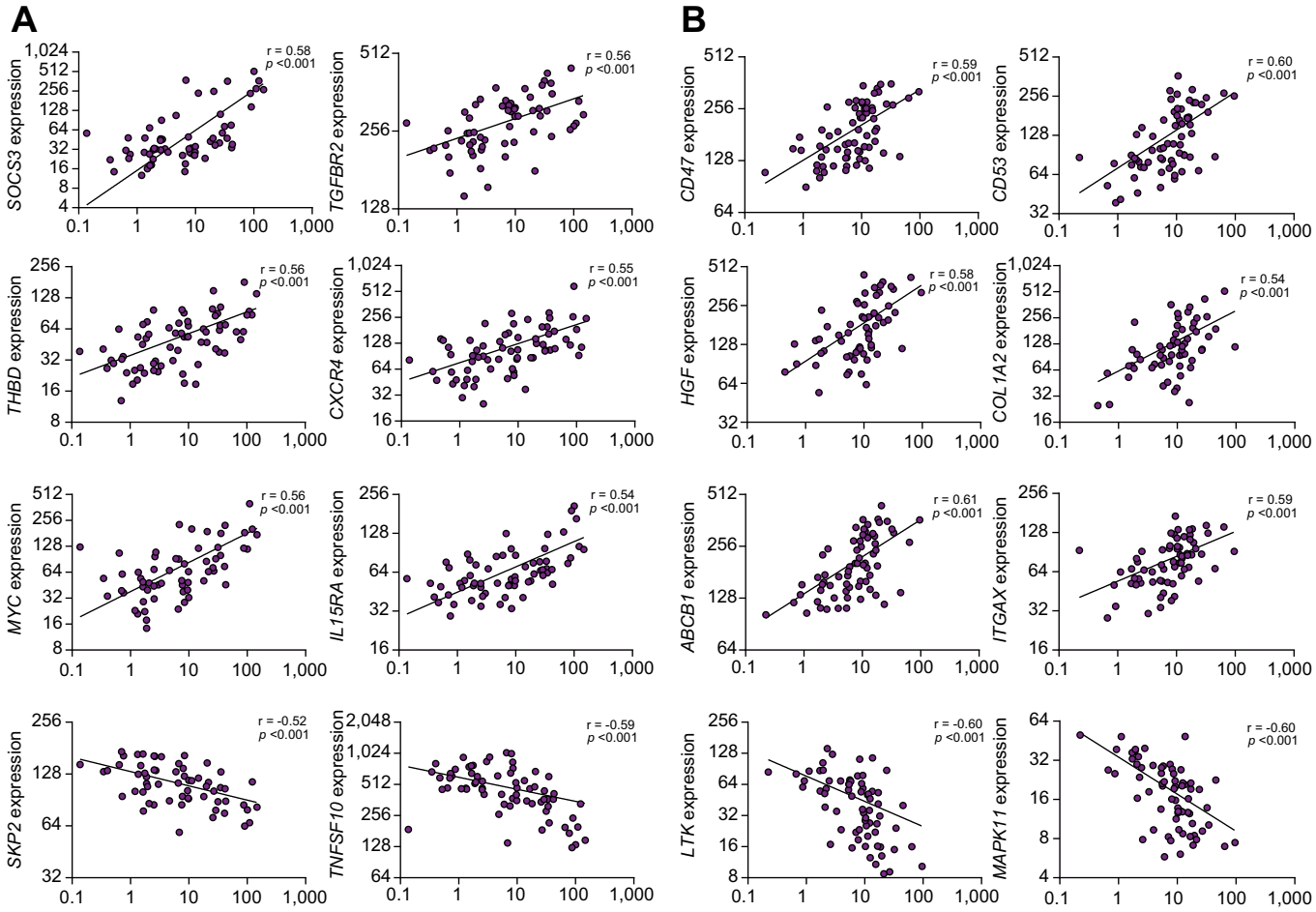

Fig. 3. Correlation between expression levels of selected genes and pSTAT3 scores. (A) With hepatocytes pSTAT3 scores. (B) With non-hepatocytes pSTAT3 scores. r, Spearman's correlation coefficient. Log10-transformed pSTAT3 scores and log2-transformed gene expression data were used. pSTAT3, phospho-STAT3.

(Table S2, Fig. 3). In hepatocytes, a strong positive correlation (r >0.5, p <0.001) was observed for TGF beta receptor 2 (*TGFBR2*), an upstream activator of STAT3, the proto-oncogene *c-MYC*, a direct target of STAT3 activation, thrombomodulin (*THBD*), C-X-C motif chemokine receptor 4 (*CXCR4*/*CD184*), interleukin 15 receptor A (*IL15*RA), IL1 receptor-associated kinase 3 (*IRAK3*), suppressor of cytokine signaling 1 and 3 (*SOCS1, SOCS3*), interferon-gamma receptor 1 (*IFNGR1*), fibroblast growth factor receptor 1 (*FGFR1*) and *IL4R*. Other upstream activators of STAT3 or direct downstream targets of STAT3 activation that positively correlated with pSTAT3 scores in hepatocytes are marked in Table S2. In non-hepatocyte areas, a strong positive correlation (r >0.5, p <0.001) was observed for 48 genes, including the direct downstream targets of STAT3 activation: Bcl-2 and hepatocyte growth factor (*HGF*), the upstream activators of STAT3: platelet-derived growth factor receptor beta (*PDGFRB*), colony stimulating factor 1 (*CSF1*) and the proto-oncogene *LYN*, the collagens *COL1A2, COL3A1* and *COL5A2*, the integrins *ITGA5, ITGA9*, *ITGAX* and *ITGB1*, hepatic progenitor cell markers: activated leukocyte cell adhesion molecule (*ALCAM*), osteopontin (*SPP1*) and interleukin enhancer binding factor 3 (*ILF3*), genes involved in TGFβ1 pathway: SMAD family member 2 (*SMAD2*), the proto-oncogene *ETS1*, insulin-like growth factor II (IGFR2), C-X-C motif chemokine ligand 6 (CXCL6) and galectin-3 (*LGALS3*), cell surface markers *CD46*, *CD47*, *CD53*, *CD58* and *CD9*, pro-fibrotic chemokines: *CXCL10* and *CXCL12*, and the endothelial marker *PECAM1*. Other upstream activators of STAT3 that positively correlated with non-hepatocyte pSTAT3 scores are marked in Table S2.

A similar analysis was performed for genes that negatively correlated with pSTAT3 scores. A total of 62 genes and 283 genes negatively correlated with hepatocyte and non-hepatocyte pSTAT3 scores, respectively, including 32 genes in common (Table S3, Fig. 3). In hepatocytes, strong negative correlations (r <-0.5, p <0.001) were observed for S-phase kinase-associated protein 2 (*SKP2*) and TNF superfamily member 10 (*TNFSF10*/*TRAIL*). In non-hepatocyte areas, strong negative correlations (r <-0.5, p <0.001) were observed for 30 genes, including cell surface markers CEACAM8/CD66b and CD160, interleukins *IL10, IL12A, IL15, IL23A* and *IL27*, TIR domain-containing adaptor protein (*TIRAP*), leukocyte receptor tyrosine kinase (*LTK*), ETS transcription factor *ELK1*, and interferon-regulatory factors *IRF3* and *IRF7*.

IPA analysis confirmed that genes associated with STAT3 activation in non-hepatocyte areas were strongly enriched in the hepatic fibrosis signaling pathway ($p = 2.0\text{x}10^{-85}$). Other enriched canonical pathways associated with STAT3 activation in non-hepatocyte areas were PI3K/AKT signaling ($p = 3.2\text{x}10^{-58}$); macrophages, fibroblasts, and endothelial cells in inflammation ($p = 2.5\text{x}10^{-66}$); Th1 and Th2 activation pathway ($p = 5.0\text{x}10^{-52}$);

Table 1. IPA identified top canonical pathways and upstream regulators from pSTAT3-correlated genes in non-hepatocyte areas.

Canonical pathways	*p* values
Hepatic fibrosis signaling pathway	2.0×10^{-85}
Macrophages, fibroblasts and endothelial cells in inflammation	2.5×10^{-66}
Glucocorticoid receptor signaling	2.0×10^{-63}
PI3K/AKT signaling	3.2×10^{-58}
Epithelial-mesenchymal transition	1.0×10^{-52}
Th1 and Th2 activation pathway	5.0×10^{-52}
Pattern recognition receptors (bacteria and viruses)	2.0×10^{-49}
PTEN signaling	4.0×10^{-49}
PKR in interferon induction and antiviral response	3.2×10^{-46}
Tumor microenvironment pathway	2.5×10^{-44}
Natural killer cell signaling	6.3×10^{-44}
Senescence pathway	4.0×10^{-43}
Upstream regulators	
IFNG	1.5×10^{-72}
TNF	1.6×10^{-69}
TGFB1	2.3×10^{-58}
IL2	1.4×10^{-52}
IL10	2.8×10^{-51}
CDKN2A	3.8×10^{-47}
CD3	2.4×10^{-46}
NR3C1	3.5×10^{-45}
NFkB	2.2×10^{-42}
STAT3	1.0×10^{-40}
IL17A	1.4×10^{-39}
CSF1	5.8×10^{-39}
STAT1	6.5×10^{-39}
IL4	1.1×10^{-38}
IL6	1.9×10^{-38}

Statistical significance was calculated using a right-tailed Fisher's exact test.
IPA, Ingenuity® Pathway Analysis.

PTEN signaling ($p = 4.0\text{x}10^{-49}$); epithelial-mesenchymal transition ($p = 1.0\text{x}10^{-52}$); and natural killer cell signaling ($6.3\text{x}10^{-44}$) (Table 1). Upstream regulators included in addition to STAT3, TNF ($p = 1.6\text{x}10^{-69}$), IFNγ ($p = 1.5\text{x}10^{-72}$), TGFβ1 ($p = 2.3\text{x}10^{-58}$), IL-2 ($p = 1.4\text{x}10^{-52}$), IL10 ($p = 2.8\text{x}10^{-51}$), CDKN2A ($p = 3.8\text{x}10^{-47}$), CD3 ($p = 2.4\text{x}10^{-46}$), NR3C1 ($p = 3.5\text{x}10^{-45}$), IL-17A ($p = 1.4\text{x}10^{-39}$), IL-4 ($p = 1.1\text{x}10^{-38}$), and IL6 ($p = 1.9\text{x}10^{-38}$) (Table 1).

Digital spatial transcriptome profiling of hepatocyte and non-hepatocyte areas segmented by pSTAT3 staining

Spatial transcriptomic profiling was performed on 13 ROIs from four NAFLD liver biopsies with advanced fibrosis, using a custom panel of morphology markers composed of pSTAT3, PanCK+CK8/18, and CD45 (Fig. 4A). The 13 ROIs were further segmented based on pSTAT3-positive or -negative staining. Following normalization and filtering by limit of quantitation, expression data were obtained for 13,174 genes. Principal component analysis plots showed a clear separation between hepatocyte and non-hepatocyte areas (Fig. 4B). While pSTAT3$^+$ and pSTAT3$^-$ cells within these areas did not fully separate, their expression profiles were still significantly different ($p < 0.001$).

Cell deconvolution analysis using an adult liver matrix estimated cell type distribution in pSTAT3$^+$ and pSTAT3$^-$ hepatocyte areas (Fig. 5A). As anticipated, hepatocytes were the main cell type with no significant change between pSTAT3$^+$ and pSTAT3$^-$ (81.3% *vs.* 82.2%). Similarly, no difference was observed for hepatic stellate cells (HSCs) (3.0% in pSTAT3$^+$ and 3.7% in pSTAT3$^-$). In contrast, the proportion of hepatic progenitor cells (HPCs) was significantly higher in pSTAT3$^+$ hepatocyte areas (1.2%) compared to pSTAT3$^-$ hepatocyte areas (0.15%) (fold change [FC] 8.0,

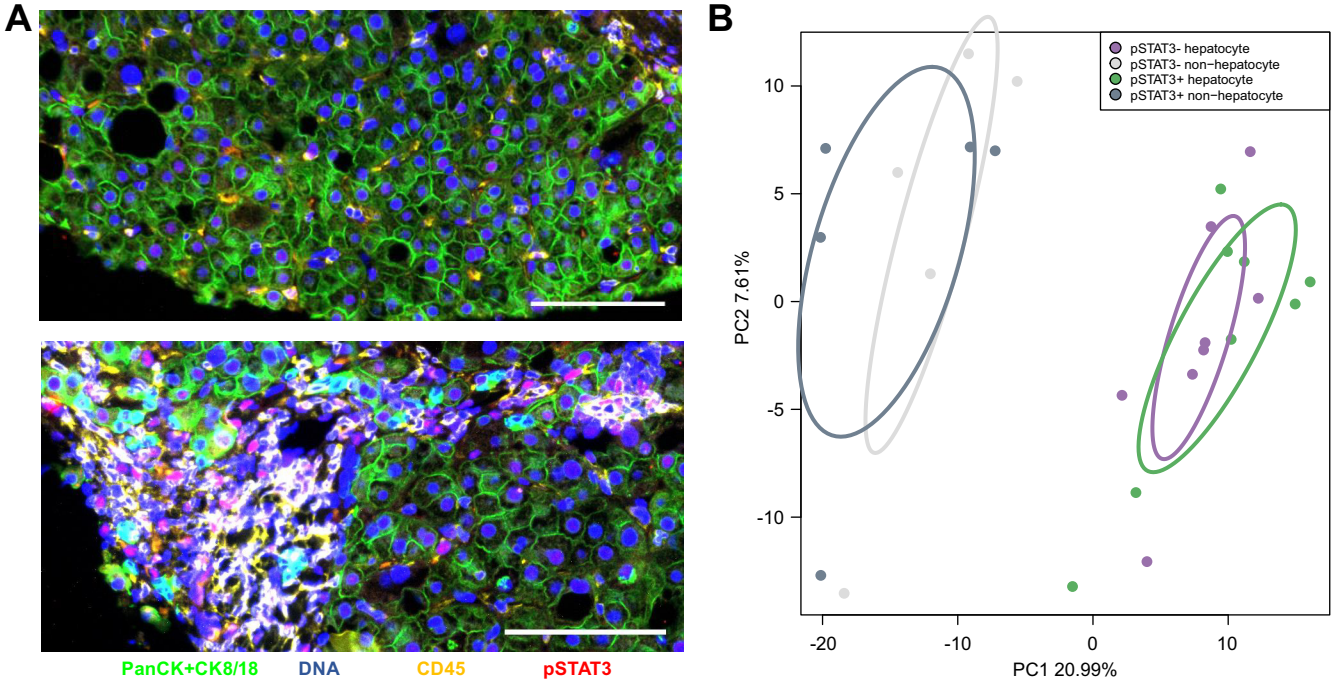

Fig. 4. Digital spatial transcriptome profiling of ROIs from NASH liver biopsies with advanced fibrosis. (A) Representative ROIs using the following color fluorescence: panCK+CK8/18 (cyan), CD45 (yellow), pSTAT3 (red), and DNA (blue) in hepatocytes (top) and non-hepatocyte/hepatocyte areas (bottom). Scale bar, 100 μm. (B) PCoA of gene expression data from whole transcriptome atlas based on hepatocyte and non-hepatocyte areas and pSTAT3 staining. Ellipses were drawn using the standard deviation of point scores. Log_{10}-transformed gene expression data were used. NASH, non-alcoholic steatohepatitis; PC, principle component; PCoA, principle component analysis; pSTAT3, phospho-STAT3; ROI, region of interest.

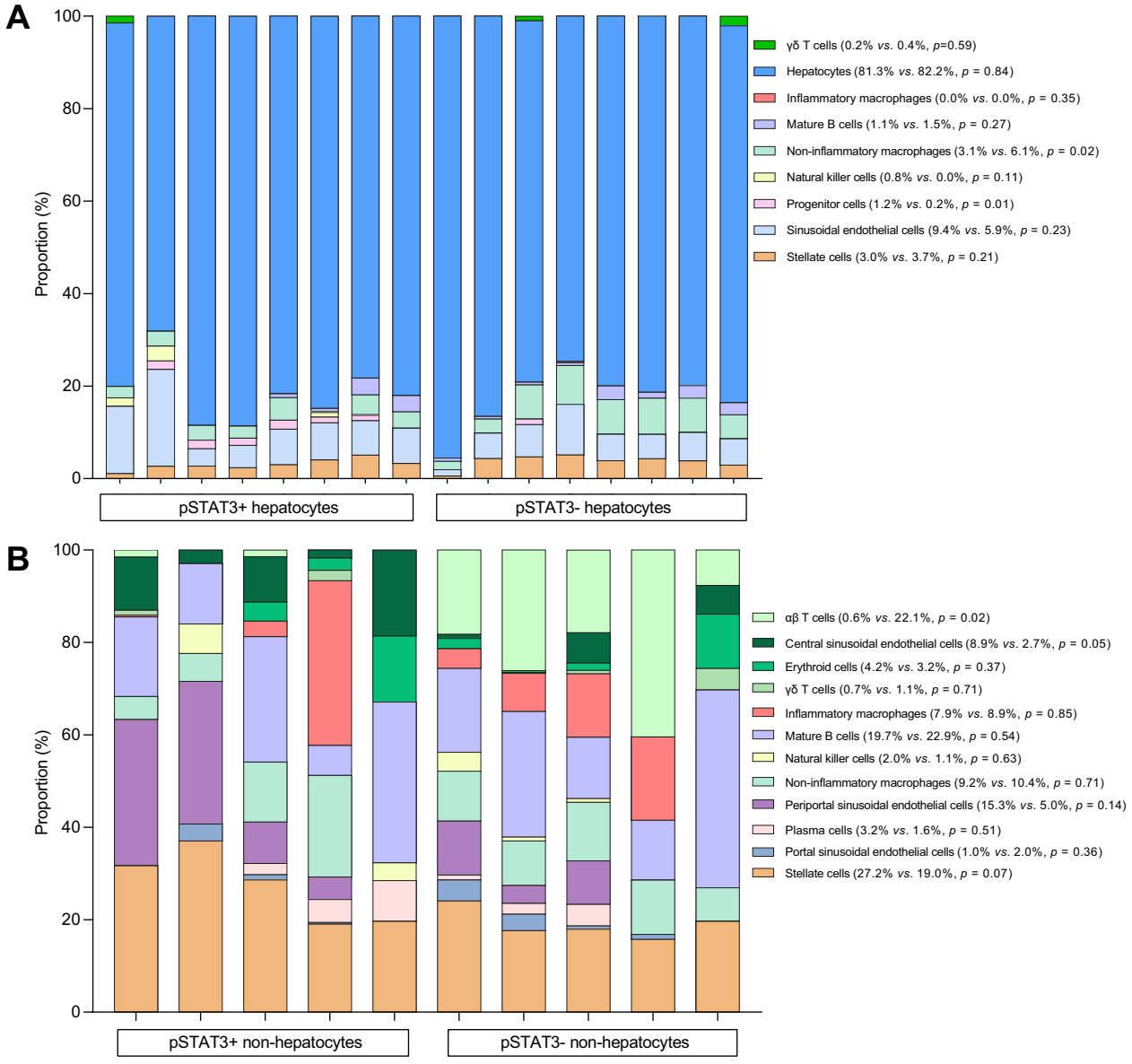

Fig. 5. Cell deconvolution plots using adult liver matrix and ROI transcriptome profiles show changes of cell proportions. In (A) hepatocyte and (B) non-hepatocyte areas. The mean of each cell proportion was calculated for hepatocyte and non-hepatocyte areas. Statistical significance was calculated using an unpaired *t* test. ROI, region of interest.

p = 0.006). Central venous sinusoidal endothelial cells (SECs) were also enriched in pSTAT3$^+$ hepatocyte areas (9.4%) compared to pSTAT3$^-$ hepatocyte areas (5.9%), although not significantly. Central venous SECs were significantly enriched in pSTAT3$^+$ non-hepatocyte areas (8.9%) compared to pSTAT3$^-$ non-hepatocyte areas (2.7%) (FC = 3.3, p = 0.048) (Fig. 5B). Periportal SECs were also enriched in pSTAT3$^+$ non-hepatocyte areas compared to pSTAT3$^-$ non-hepatocyte areas (15.3% *vs.* 5%), although not significantly. For immune cells, αβ T cells were significantly depleted in pSTAT3$^+$ non-hepatocyte areas (0.6% *vs.* 22.1%, FC = -36.7, p = 0.018), suggesting no detection of pSTAT3 in these cells. pSTAT3 was detected but not significantly enriched in γδ T cells, Kupffer cells (inflammatory and non-inflammatory macrophages), mature B cells, natural killer cells and plasma B cells (Fig. 5B).

Cell distribution changes in mouse NASH livers upon STAT3 inhibition

To determine whether STAT3 activation contributed to self-renewal of HPCs or liver SECs in NASH livers, cell deconvolution analysis using a mouse liver matrix was performed on transcriptomic profiles we previously reported,[19] from NASH livers of Hep*Pten*$^-$ mice treated for 4 weeks with C188-8, a STAT3 inhibitor, or placebo. While no difference was observed for liver SECs (8.1% *vs.* 8.7%), HPCs were significantly depleted upon C188-9 treatment (3.7% *vs.* 5.8%) (FC = -1.6, p = 0.048) (Fig. 6). Kupffer cells (2.7% *vs.* 5.4%; FC = -2.0, p <0.001) and plasmacytoid dendritic cells (0.5% *vs.* 1.8%; FC = -3.6, p <0.001) were also depleted upon C188-8 treatment. In addition, while the overall percentage of hepatocytes was unchanged, C188-9 treatment resulted in the reduction of pericentral hepatocytes (30.1% *vs.* 38.6%) (FC = -1.3, p

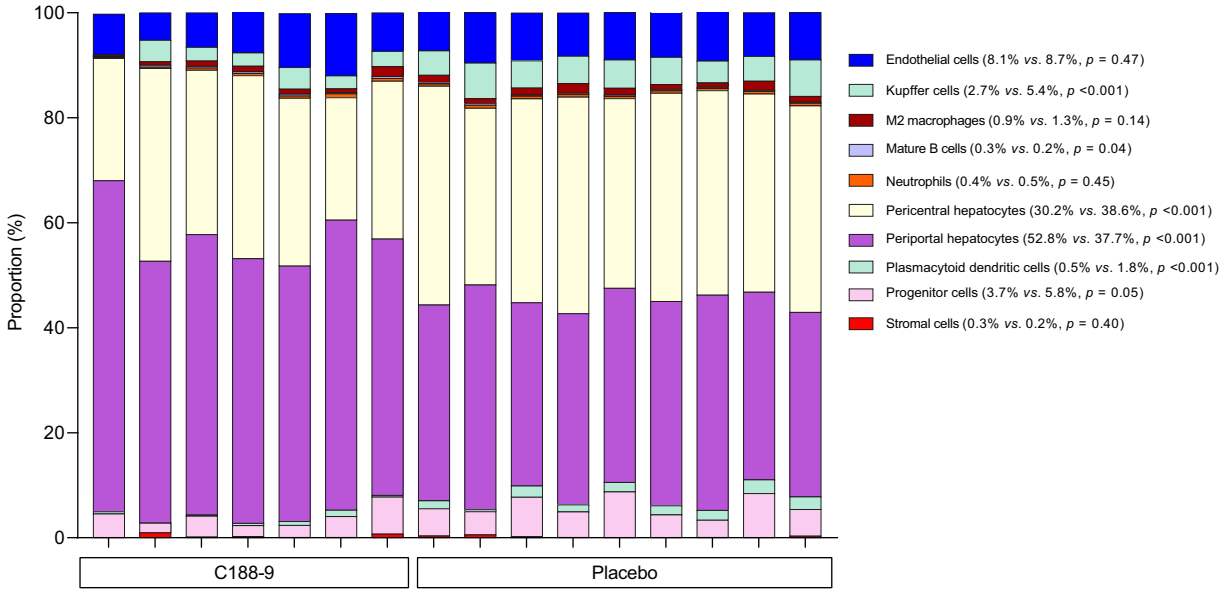

Fig. 6. Cell deconvolution analysis using mouse liver matrix and transcriptomic profiles show changes of cell proportions in NASH livers between Hep*Pten*$^{-}$ mice treated with C188-9 or placebo. The mean of each cell proportion was calculated for treated mice and placebo. Statistical significance was calculated using an unpaired *t* test. NASH, non-alcoholic steatohepatitis.

<0.001) and concomitant expansion of periportal hepatocytes (52.6% *vs.* 37.7%) (FC = 1.4, p <0.001).

Discussion

STAT3 is strongly associated with liver injury, inflammation, regeneration, and HCC development.[23,24] We have also reported a role of STAT3 in liver fibrosis in mice.[17] While it was suggested that STAT3 signaling drives HSC activation to promote liver fibrosis,[25,26] molecular and cellular spatial studies of STAT3 in human NASH are lacking. Herein, we demonstrated that STAT3 activation strongly correlates with liver fibrosis severity in patients with NAFLD. The correlation was stronger for STAT3 activation in cells other than hepatocytes.

A major role of STAT3 activation on hepatic fibrosis was further confirmed by IPA of genes whose expression correlated with STAT3 activation in non-hepatocyte areas. Very strong positive correlations with STAT3 activation were observed for several collagens (*COL1A2, COL3A1, COL5A2*), integrins (*ITGA5, ITGA9, ITGAX, ITGB1*), and pro-fibrotic chemokines (*CXCL10, CXCL12*). IPA also suggested that activation of TGFβ signaling was a major mediator of pro-fibrotic STAT3 activity. Indeed, strong correlations were observed with many genes in this pathway, including *TGFBR2, SMAD2, ETS1, IGFR2, CXCL6*, and galectin-3. Aberrant TGFβ signaling in conjunction with trans-differentiation of HSCs into fibrogenic myofibroblasts plays a central role in liver fibrosis.[27] SMAD proteins are pivotal intracellular effectors of TGFβ in hepatic fibrosis.[28] Galectin-3 is upregulated in human fibrotic liver disease.[29] In galectin-3 null mice, hepatic fibrosis following liver injury is reduced and TGFβ fails to activate HSCs.[30] It has been previously reported that cooperation of STAT3 and TGFβ1 in HSCs exacerbates liver injury and fibrosis[31] and that STAT3 activation is essential for TGFβ activation of HSCs.[32–34] In our study, STAT3 activation was detected in approximately half of the HSCs and this activation was not required for their proliferation or survival. Future experiments should further characterize these two HSC subpopulations.

Two cell surface markers that strongly correlated with STAT3 activation in non-hepatocyte areas were the tetraspanin CD9 and the innate immune regulator CD47. Anti-CD47 antibody treatment attenuates liver inflammation and fibrosis in NASH mouse models.[35] CD9 is an important cell surface marker associated with liver fibrosis. Single-cell analysis of cirrhotic livers identified a scar-associated TREM2^{+}CD9^{+} subpopulation of macrophages, which expands in liver fibrosis and is pro-fibrogenic.[36]

In non-hepatocyte areas, strong negative correlations with STAT3 activation were observed for IL-10 and IL-15, two major anti-inflammatory and anti-fibrotic cytokines in the liver. IL-10 was also found as an upstream regulator by IPA, suggesting an important role in STAT3-mediated liver fibrosis. Mesenchymal stem cells overexpressing IL-10 inhibited liver fibrosis in mice.[37] Growing evidence suggests an important role of B cells in the development of NAFLD. B cell harboring but antibody-deficient IgMi mice were completely protected from the development of hepatic steatosis, inflammation, and fibrosis upon a high-fat diet (HFD) feeding. HFD reduced the number of regulatory B cells and IL-10 production in the liver.[38]

We found a strong correlation between expression of the endothelial cell marker PECAM1 and STAT3 activation in non-hepatocyte areas. Digital spatial profiling confirmed strong levels of activated STAT3 in liver SECs (LSECs). LSECs are known actors in the fibrogenic response to injury. Activated HSCs, LSECs, and Kupffer cells are responsible for sinusoidal capillarization and perisinusoidal matrix deposition, promoting fibrogenesis.[39,40] STAT3 activation also strongly correlated with the expression of HPC markers such as ALCAM, SPP1, ILF3, and CXCR4/CD184. Interestingly, activated STAT3 was specifically enriched in HPCs as shown by digital spatial profiling, suggesting that STAT3 activation may lead to either dedifferentiation of

hepatocytes or increased cell expansion of HPCs. In the context of HCC, several studies have reported that STAT3 signaling promotes the expansion of tumor-initiating cell self-renewal and increases the stemness of HCC stem cells.[41–45]

To determine whether STAT3 activation contributes to HPC and LSEC expansion in NASH livers, we performed deconvolution analysis using a mouse adult liver matrix of transcriptomic data we previously generated on the liver from Hep*Pten*$^{-}$ mice treated for four weeks with C188-9, a STAT3 inhibitor, or placebo.[17] This analysis revealed that C188-9 treatment results in depletion of HPCs, demonstrating that STAT3 activation in HPCs induces their expansion. We and others previously showed that the proliferation of HPCs is important in HSC activation. It was suggested that increased fibrosis likely occurs by primary progenitor expansion/proliferation and secondary fibrotic myofibroblast expansion, in close contact with progenitors.[46,47] We reported that anti-miR-21 treatment reduced liver fibrosis with a concomitant reduction of CD24+ liver progenitor cells.[48]

Kupffer cells and plasmacytoid dendritic cells were also depleted upon C188-8 treatment. The Kupffer cells, labeled as inflammatory and non-inflammatory macrophages in the human liver matrix, we used for deconvolution analysis were not enriched for pSTAT3 in the human liver biopsies. Plasmacytoid dendritic cells were not represented in the human liver matrix. Major limitations of the analysis of immune cells are the lack of canonical markers and standardized classification of immune cells in the liver. Translating mice immune cell data to humans is also challenging. Finally, there is only partial overlap of the immune cells included in the currently available human and mouse liver matrices.

While the overall percentage of hepatocytes was unchanged, C188-9 treatment resulted in the reduction of pericentral hepatocytes and concomitant expansion of periportal hepatocytes. Certain liver injuries are zone-dependent, with NAFLD for example, originating in pericentral regions of the lobule in adults.[49] NAFLD and NASH/cirrhosis initially develop in pericentral cells and progress toward periportal regions. Pericentral hepatocytes have increased expression of HPC markers and can replace most hepatocytes in the lobule during homeostatic renewal. LSECs in pericentral regions are also more susceptible to damage associated with cirrhosis compared to periportal LSECs.

Whether these findings are specific to patients with NAFLD or reflect a general mechanism of disease progression should be investigated in follow-up studies. Understanding in particular, the common and distinct molecular and cellular determinants of liver fibrosis progression in the context of NAFLD, alcoholic steatohepatitis and viral hepatitis, would be highly valuable.

This study strongly increases our understanding of the spatial dependence of main signaling pathways such as STAT3 in NASH and liver fibrosis progression. It also increases our understanding of the role of specific cell types, such as HPCs, in liver fibrosis progression. Such information could improve targeted treatment approaches. In addition, future digital spatial profiler experiments would benefit from using different sets of liver cell type markers, such as HSC, HPC and SEC markers.

Abbreviations

DSP, digital spatial profiler; FC, fold change; HCC, hepatocellular carcinoma; HFD, high-fat diet; HPCs, hepatic progenitor cells; HSCs, hepatic stellate cells; IPA, Ingenuity® Pathway Analysis; LSECs, liver sinusoidal endothelial cells; NAFLD, non-alcoholic fatty liver disease; NAS, NAFLD activity score; NASH, non-alcoholic steatohepatitis; pSTAT3, phospho-STAT3; SECs, sinusoidal endothelial cells; STAT, signal transducer and activator of transcription.

Financial support

This study was supported in part by NIH/NCI R01 CA195524 to L. Beretta and by the MD Anderson Cancer Center support grant CA016672.

Conflict of interest

The authors declare no conflicts of interest that pertain to this work.

Please refer to the accompanying ICMJE disclosure forms for further details.

Authors' contributions

J.J. and J.I.S. were responsible for the study concept and design, acquisition of data, interpretation of data, drafting of the manuscript, and statistical analysis; O.S. and H.L.S. were responsible for the collection of samples; L.M.S., D.J.T., and D.M.M. were responsible for technical support; L.B was responsible for study concept and design, interpretation of data, drafting of the manuscript, obtaining funding and study supervision.

Data availability statement

All data relevant to the study are included in the article or uploaded as Supplementary Material.

Acknowledgments

The authors would like to thank for their technical assistance, Ms. Haidee Chancoco from the MD Anderson Cancer Center Biospecimen Extraction Facility, Ms. Indu Raman from the Microarray Core Facility at The University of Texas Southwestern, Dr. Liang Zhang from Nanostring Technologies Inc., Mr. Victor Ortega, Director of the Immunohistochemistry laboratory in the Department of Pathology at MD Anderson Cancer Center as well as Drs. Sharia Hernandez, Frank Rojas Alvarez, and Wei Lu in the Department of Translational Molecular Pathology at MD Anderson Cancer Center.

Supplementary data

Supplementary data to this article can be found online at https://doi.org/10.1016/j.jhepr.2022.100628.

References

Author names in bold designate shared co-first authorship.

[1] Younossi ZM, Stepanova M, Younossi Y, Golabi P, Mishra A, Rafiq N, et al. Epidemiology of chronic liver diseases in the USA in the past three decades. Gut 2020;69:564–568.
[2] Younossi ZM, Stepanova M, Ong J, Trimble G, AlQahtani S, Younossi I, et al. Nonalcoholic steatohepatitis is the most rapidly increasing indication for liver transplantation in the United States. Clin Gastroenterol Hepatol 2021;19:580–589 e585.
[3] Lee YA, Friedman SL. Inflammatory and fibrotic mechanisms in NAFLD-Implications for new treatment strategies. J Intern Med 2022;291:11–31.
[4] Powell EE, Wong VW, Rinella M. Non-alcoholic fatty liver disease. Lancet 2021;397:2212–2224.
[5] Taylor RS, Taylor RJ, Bayliss S, Hagstrom H, Nasr P, Schattenberg JM, et al. Association between fibrosis stage and outcomes of patients with nonalcoholic fatty liver disease: a systematic review and meta-analysis. Gastroenterology 2020;158:1611–1625 e1612.
[6] Dulai PS, Singh S, Patel J, Soni M, Prokop LJ, Younossi Z, et al. Increased risk of mortality by fibrosis stage in nonalcoholic fatty liver disease: systematic review and meta-analysis. Hepatology 2017;65:1557–1565.
[7] Noureddin M, Ntanios F, Malhotra D, Hoover K, Emir B, McLeod E, et al. Predicting NAFLD prevalence in the United States using National Health and Nutrition Examination Survey 2017-2018 transient elastography data

and application of machine learning. Hepatol Commun 2022;6(7):1537–1548.
[8] Johnston PA, Grandis JR. STAT3 signaling: anticancer strategies and challenges. Mol Interv 2011;11:18–26.
[9] Carpenter RL, Lo HW. STAT3 target genes relevant to human cancers. Cancers 2014;6:897–925.
[10] Wang H, Lafdil F, Kong X, Gao B. Signal transducer and activator of transcription 3 in liver diseases: a novel therapeutic target. Int J Biol Sci 2011;7:536–550.
[11] Choi E, Kim W, Joo SK, Park S, Park JH, Kang YK, et al. Expression patterns of STAT3, ERK and estrogen-receptor alpha are associated with development and histologic severity of hepatic steatosis: a retrospective study. Diagn Pathol 2018;13:23.
[12] Su TH, Shiau CW, Jao P, Liu CH, Liu CJ, Tai WT, et al. Sorafenib and its derivative SC-1 exhibit antifibrotic effects through signal transducer and activator of transcription 3 inhibition. Proc Natl Acad Sci United States America 2015;112:7243–7248.
[13] Horiguchi N, Ishac EJ, Gao B. Liver regeneration is suppressed in alcoholic cirrhosis: correlation with decreased STAT3 activation. Alcohol 2007;41:271–280.
[14] Yang SF, Wang SN, Wu CF, Yeh YT, Chai CY, Chunag SC, et al. Altered p-STAT3 (tyr705) expression is associated with histological grading and intratumour microvessel density in hepatocellular carcinoma. J Clin Pathol 2007;60:642–648.
[15] **Liang C**, **Xu Y**, Ge H, Li G, Wu J. Clinicopathological significance and prognostic role of p-STAT3 in patients with hepatocellular carcinoma. OncoTargets Ther 2018;11:1203–1214.
[16] Grohmann M, Wiede F, Dodd GT, Gurzov EN, Ooi GJ, Butt T, et al. Obesity drives STAT-1-dependent NASH and STAT-3-dependent HCC. Cell 2018;175:1289–1306 e1220.
[17] Jung KH, Yoo W, Stevenson HL, Deshpande D, Shen H, Gagea M, et al. Multifunctional effects of a small-molecule STAT3 inhibitor on NASH and hepatocellular carcinoma in mice. Clin Cancer Res : official J Am Assoc Cancer Res 2017;23:5537–5546.
[18] Wang Z, Li J, Xiao W, Long J, Zhang H. The STAT3 inhibitor S3I-201 suppresses fibrogenesis and angiogenesis in liver fibrosis. Lab Invest 2018;98:1600–1613.
[19] Kleiner DE, Brunt EM, Van Natta M, Behling C, Contos MJ, Cummings OW, et al. Design and validation of a histological scoring system for nonalcoholic fatty liver disease. Hepatology 2005;41:1313–1321.
[20] Perkins JR, Dawes JM, McMahon SB, Bennett DL, Orengo C, Kohl M. ReadqPCR and NormqPCR: R packages for the reading, quality checking and normalisation of RT-qPCR quantification cycle (Cq) data. BMC Genomics 2012;13:296.
[21] MacParland SA, Liu JC, Ma XZ, Innes BT, Bartczak AM, Gage BK, et al. Single cell RNA sequencing of human liver reveals distinct intrahepatic macrophage populations. Nat Commun 2018;9:4383.
[22] Han X, Wang R, Zhou Y, Fei L, Sun H, Lai S, et al. Mapping the mouse cell atlas by microwell-seq. Cell 2018;172:1091–1107 e1017.
[23] **Hu Z**, **Han Y**, Liu Y, Zhao Z, Ma F, Cui A, et al. CREBZF as a key regulator of STAT3 pathway in the control of liver regeneration in mice. Hepatology 2020;71:1421–1436.
[24] He G, Karin M. NF-kappaB and STAT3 - key players in liver inflammation and cancer. Cel Res 2011;21:159–168.
[25] Meng F, Wang K, Aoyama T, Grivennikov SI, Paik Y, Scholten D, et al. Interleukin-17 signaling in inflammatory, Kupffer cells, and hepatic stellate cells exacerbates liver fibrosis in mice. Gastroenterology 2012;143:765–776 e763.
[26] **Xiang DM**, **Sun W**, **Ning BF**, Zhou TF, Li XF, Zhong W, et al. The HLF/IL-6/STAT3 feedforward circuit drives hepatic stellate cell activation to promote liver fibrosis. Gut 2018;67:1704–1715.
[27] Fabregat I, Caballero-Diaz D. Transforming growth factor-beta-induced cell plasticity in liver fibrosis and hepatocarcinogenesis. Front Oncol 2018;8:357.
[28] Xu F, Liu C, Zhou D, Zhang L. TGF-beta/SMAD pathway and its regulation in hepatic fibrosis. J Histochem Cytochem : official J Histochem Soc 2016;64:157–167.
[29] Henderson NC, Mackinnon AC, Farnworth SL, Poirier F, Russo FP, Iredale JP, et al. Galectin-3 regulates myofibroblast activation and hepatic fibrosis. Proc Natl Acad Sci United States America 2006;103:5060–5065.
[30] Jeftic I, Jovicic N, Pantic J, Arsenijevic N, Lukic ML, Pejnovic N. Galectin-3 ablation enhances liver steatosis, but attenuates inflammation and IL-33-dependent fibrosis in obesogenic mouse model of nonalcoholic steatohepatitis. Mol Med 2015;21:453–465.
[31] Xu MY, Hu JJ, Shen J, Wang ML, Zhang QQ, Qu Y, et al. Stat3 signaling activation crosslinking of TGF-beta1 in hepatic stellate cell exacerbates liver injury and fibrosis. Biochim Biophys Acta 2014;1842:2237–2245.
[32] Liu Y, Liu H, Meyer C, Li J, Nadalin S, Konigsrainer A, et al. Transforming growth factor-beta (TGF-beta)-mediated connective tissue growth factor (CTGF) expression in hepatic stellate cells requires Stat3 signaling activation. J Biol Chem 2013;288(42):30708–30719.
[33] Tang LY, Heller M, Meng Z, Yu LR, Tang Y, Zhou M, et al. Transforming growth factor-beta (TGF-beta) directly activates the JAK1-STAT3 Axis to induce hepatic fibrosis in coordination with the SMAD pathway. J Biol Chem 2017;292(10):4302–4312.
[34] Cierpka R, Weiskirchen R, Asimakopoulos A. Perilipin 5 ameliorates hepatic stellate cell activation via SMAD2/3 and SNAIL signaling pathways and suppresses STAT3 activation. Cells 2021;10(9):2184.
[35] Gwag T, Ma E, Zhou C, Wang S. Anti-CD47 antibody treatment attenuates liver inflammation and fibrosis in experimental non-alcoholic steatohepatitis models. Liver Int 2022;42:829–841.
[36] Ramachandran P, Dobie R, Wilson-Kanamori JR, Dora EF, Henderson BEP, Luu NT, et al. Resolving the fibrotic niche of human liver cirrhosis at single-cell level. Nature 2019;575:512–518.
[37] Choi JS, Jeong IS, Han JH, Cheon SH, Kim SW. IL-10-secreting human MSCs generated by TALEN gene editing ameliorate liver fibrosis through enhanced anti-fibrotic activity. Biomater Sci 2019;7:1078–1087.
[38] Karl M, Hasselwander S, Zhou Y, Reifenberg G, Kim YO, Park KS, et al. Dual roles of B lymphocytes in mouse models of diet-induced nonalcoholic fatty liver disease. Hepatology 2022;76(4):1135–1149.
[39] Terkelsen MK, Bendixen SM, Hansen D, Scott EAH, Moeller AF, Nielsen R, et al. Transcriptional dynamics of hepatic sinusoid-associated cells after liver injury. Hepatology 2020;72:2119–2133.
[40] Ramirez-Pedraza M, Fernandez M. Interplay between macrophages and angiogenesis: a double-edged sword in liver disease. Front Immunol 2019;10:2882.
[41] Wan S, Zhao E, Kryczek I, Vatan L, Sadovskaya A, Ludema G, et al. Tumor-associated macrophages produce interleukin 6 and signal via STAT3 to promote expansion of human hepatocellular carcinoma stem cells. Gastroenterology 2014;147:1393–1404.
[42] Chen ZZ, Huang L, Wu YH, Zhai WJ, Zhu PP, Gao YF. LncSox4 promotes the self-renewal of liver tumour-initiating cells through Stat3-mediated Sox4 expression. Nat Commun 2016;7:12598.
[43] Wang X, Sun W, Shen W, Xia M, Chen C, Xiang D, et al. Long non-coding RNA DILC regulates liver cancer stem cells via IL-6/STAT3 axis. J Hepatol 2016;64:1283–1294.
[44] Won C, Kim BH, Yi EH, Choi KJ, Kim EK, Jeong JM, et al. Signal transducer and activator of transcription 3-mediated CD133 up-regulation contributes to promotion of hepatocellular carcinoma. Hepatology 2015;62:1160–1173.
[45] Uthaya Kumar DB, Chen CL, Liu JC, Feldman DE, Sher LS, French S, et al. TLR4 signaling via NANOG cooperates with STAT3 to activate Twist1 and promote formation of tumor-initiating stem-like cells in livers of mice. Gastroenterology 2016;150:707–719.
[46] Greenbaum LE, Wells RG. The role of stem cells in liver repair and fibrosis. Int J Biochem Cel Biol 2011;43:222–229.
[47] Grzelak CA, Martelotto LG, Sigglekow ND, Patkunanathan B, Ajami K, Calabro SR, et al. The intrahepatic signalling niche of hedgehog is defined by primary cilia positive cells during chronic liver injury. J Hepatol 2014;60:143–151.
[48] Zhang J, Jiao J, Cermelli S, Muir K, Jung KH, Zou R, et al. miR-21 inhibition reduces liver fibrosis and prevents tumor development by inducing apoptosis of CD24+ progenitor cells. Cancer Res 2015;75:1859–1867.
[49] Cunningham RP, Porat-Shliom N. Liver zonation - revisiting old questions with new technologies. Front Physiol 2021;12:732929.